METEOROLOGICAL APPLICATIONS
Meteorol. Appl. **22**: 301–313 (2015)
Published online 9 May 2014 in Wiley Online Library
(wileyonlinelibrary.com) DOI: 10.1002/met.1455

RMetS
Royal Meteorological Society

Weather Research and Forecasting model simulations of a rare springtime bow echo near the Great Salt Lake, USA

L. Zhao,[a,b,c] S.-Y. Wang,[a,d]* J. Jin[a,b] and A. J. Clark[e,f]

[a] *Department of Plants, Soils, and Climate, Utah State University, Logan, UT, USA*
[b] *Department of Watershed Sciences, Utah State University, Logan, UT, USA*
[c] *Key Laboratory of Land Surface Process and Climate Change in Cold and Arid Regions, Cold and Arid Regions Environmental and Engineering Research Institute, Chinese Academy of Sciences, Lanzhou, China*
[d] *Utah Climate Center, Utah State University, Logan, UT, USA*
[e] *Cooperative Institute for Mesoscale Meteorological Studies, University of Oklahoma, Norman, OK, USA*
[f] *NOAA/OAR National Severe Storms Laboratory, Norman, OK, USA*

ABSTRACT: The semiarid climate and rugged terrain in the interior west of the United States do not favour the development of bow echoes, a type of convective storm associated with intense, damaging winds. However, on 21 April 2011, a bow echo associated with a fast-moving midtropospheric perturbation formed across the Great Salt Lake (GSL) in Utah, producing damaging winds along its path. Intrigued by the rarity of this bow echo and the inability of the North American Mesoscale model (NAM) to forecast it, this event was studied by using available observations and conducted simulations with the Advanced Research Weather Research and Forecasting (WRF) model. Sensitivity to the microphysics schemes (MPSs), horizontal grid spacing, intensity of moisture content, and a physical lake model in the WRF model were examined. It was found that: (a) reduction in grid spacing from 12 and 4 km to 1 km along with improved depiction of low-level moisture substantially improved the bow echo simulation, (b) the presence of GSL did not impact bow echo development, and (c) the WRF model appeared to inherit a phase error in the passage of the midtropospheric perturbation from the NAM initial and lateral boundary conditions. The phase error resulted in a 1–2 h delay in the bow echo passage. These results highlight the difficulties in simulating such a bow echo event, and suggest similar challenges future faced by subsequent regional climate downscaling studies on future extreme weather in the western United States.

KEY WORDS modelling; forecasting; numerical simulation; bow echo; Great Salt Lake

Received 2 April 2013; Revised 10 December 2013; Accepted 6 January 2014

1. Introduction

The term 'bow echo' describes a type of convective storm associated with intense, damaging winds and downbursts (Fujita, 1978). The dynamics, structure and associated synoptic conditions of the bow echo have been studied extensively through both observational (Funk *et al.*, 1998; Burke and Schultz, 2004; Klimowski *et al.*, 2004; Atkins and St. Laurent, 2009a,b) and numerical approaches (Weisman, 1993; Trapp and Weisman, 2003; Weisman and Trapp, 2003; James *et al.*, 2006). In the United States, bow echoes occur normally during spring and summer in the central and eastern plains; they occur rarely over the semiarid, rugged Intermountain West between the Cascade-Sierra Range and the Rocky Mountains. For example, Klimowski *et al.* (2004) identified only two bow echo events west of the Rocky Mountains during the period 1996–2002, although their study was not designed to be a comprehensive bow echo climatology. Examining the cold season (October–April), Burke and Schultz (2004) identified only one bow echo event during the 1997–2001 period. Additionally, only a very small number of fatalities related to non-tornadic convective wind events occurred in the western United States in the period 1998–2007 (Schoen and Ashley, 2011).

On 21 April 2011 an intense convective line formed over the Great Salt Lake (GSL) in Utah around 1900 UTC (1200 local time; Figures 1(a) and (b)) associated with a fast-moving midtropospheric short-wave trough (shown later). Radar images based on the S-band (2.7–3.0 GHz) Weather Surveillance Radar 1988 Doppler (KMTX WSR 88D) (Crum *et al.*, 1993) indicated that the convective line began organizing around 1800 UTC (Figure 1(a)) and intensified quickly within an hour of moving across the GSL (Figure 1(b)). The convective line then dissipated rapidly after encountering the Wasatch Mountains east of the GSL. The intensity and curved shape observed in radar reflectivity imagery, along with the strong damaging winds reported along the path of this system, are consistent with a bow echo. Radial velocity imagery (Figures 1(c) and (d)) also suggested that this 21 April case met clearly some of the criteria of bow echo structure (Fujita, 1978; Weisman, 1993), such as ascending front to rear inflow (Businger *et al.*, 1998). A number of stations along the eastern shore of the GSL recorded wind gusts exceeding 58 kn with maximum winds reaching 104 kn (Figure 1(e)). Therefore, this convective line is referred to as a bow echo hereafter.

Bow echo systems are extremely rare in this region during this time of the year. After examining damaging wind reports compiled by the National Climatic Data Center (NCDC)

* Correspondence: S.-Y. Wang, Department of Plants, Soils, and Climate, Utah State University, 4820 Old Main Hill, Logan, UT 84321, USA. E-mail: simon.wang@usu.edu

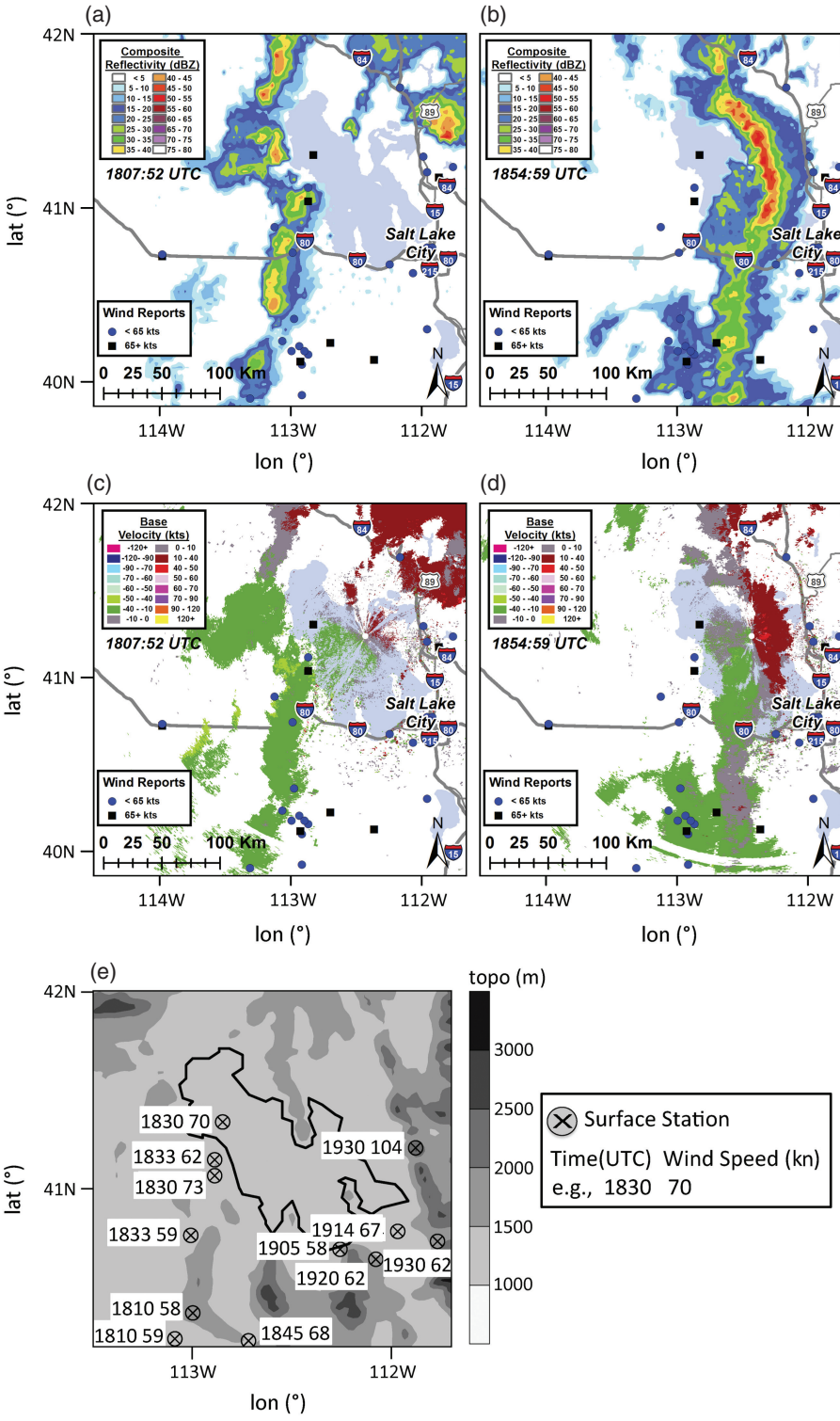

Figure 1. Observed composite reflectivity (dbz) and base velocity (kn) over the Great Salt Lake (GSL), (a) and (c) at 1807 UTC 21 April 2011, (b) and (d) at 1854 UTC 21 April 2011, respectively; (e) the corresponding severe wind reports from the Storm Prediction Center (SPC) valid 1200–1200 UTC 21–22 April 2011.

publication *Storm Data* and obtained from the Storm Prediction Center (SPC), only five records of wind speed exceeding the 'severe' threshold of 50 kn (defined by SPC) were found during April over the period 1960–2010 and within the 100 mi radius of the GSL. Past high-wind events in this area have resulted usually from intense, fast-moving cold fronts similar to those documented by Shafer and Steenburgh (2008), that is, at a larger scale, which often form in a southwesterly large-scale flow and then intensify as a mobile upper-level trough approaches from the west. In addition, examination of the radar reflectivity images archived at http://locust.mmm.ucar.edu indicates that, since 1996, there have not been any squall lines as intense as this 21 April 2011 event that occurred in the GSL area (based on reflectivity data as well as Brian McInerney

of the National Weather Service at Salt Lake City, 2011, personal communication). It is therefore not surprising that operational mesoscale forecasting models like the North American Mesoscale model (NAM) (Janjić, 2003) gave no indication of such an event, even when initialized only 6 h prior to the bow echo's occurrence (shown later).

Intrigued by the rarity of bow echoes in Utah and motivated by the inability of current mesoscale forecasting models (i.e. NAM) to simulate the 21 April case, a decision was made to study this event using the Advanced Research Weather Research and Forecasting (WRF) model (herein ARW; Shamarock *et al.*, 2008). The purpose of this study was to evaluate the performance of the ARW in simulating this unique bow echo. Case studies like this are a crucial first step in achieving reliable regional downscaling information of climate projections for this region, along with assessment of future extreme weather events. In this study, all simulations were conducted at convection-allowing spatial resolution (i.e. horizontal grid spacing $\leq$5 km with convective scheme turned off). Model experiments were designed to examine precipitation sensitivity to microphysics schemes (MPSs), horizontal grid spacing, and intensity of moisture content. In addition, the possible impact of the GSL on the bow echo development was explored; this was motivated by the apparent intensification of the bow echo as it passed over the GSL (Figures 1(a) and (b)). Finally, the impact of different initial conditions on the bow echo simulations was investigated.

The paper is arranged as follows: Section 2 describes the data source and the experiment design with the ARW; Section 3 presents the analysis and discussion of results; Section 4 provides concluding remarks.

2. Data and model settings

2.1. Data

Precipitation data used in this study were obtained from the National Centers for Environmental Prediction (NCEP) stage IV multi-sensor (radar + gauges) precipitation analyses (known as MPEs; Baldwin and Mitchell, 1997). The 13 km analyses from the NCEP Rapid Update Cycle model (RUC; Benjamin *et al.*, 2004a,b) were used for the depiction of hourly weather conditions. Radar data were obtained from the NCDC at http://www.ncdc.noaa.gov/. The NAM analyses and forecast data (12 km grid spacing) were obtained from NCDC. The NAM model runs four times daily and provides 3 h outputs. In addition, the North American Regional Analysis (NARR; 32 km grid spacing) (Mesinger *et al.*, 2006) was used for the period of 1991–2010 with the 3 h output. Finally, lake surface temperature was derived from the Moderate Resolution Imaging Spectroradiometer (MODIS) data, obtained from NASA (http://reverb.echo.nasa.gov). The daily product (MYD11C1) was used including daytime and night time surface temperature and configured onto a 0.05°latitude/longitude ($\sim$5.6 km) grid.

2.2. Simulation design

The ARW version 3.0 used here was coupled with the Community Land Model version 3.5 (CLM3.5), which includes a 10-layer physical lake scheme (Jin *et al.*, 2010). The GSL contains high salinity in northern arm (25–28% by mass) and in southern arm (8–15% by mass; Crosman and Horel, 2009), which makes the lake unfrozen almost all the time. Thus, in all experiments, the GSL was configured as an unfrozen lake to mimic the actual condition. However, other effects of salinity on the physical features of the lake water such as surface evaporation, heat capacity and thermal conductivity were not considered in the model for this study. Two sets of simulations were performed with and without the lake under different atmospheric schemes. This ARW–CLM3.5 coupled model (herein ARW for simplicity) allowed us to examine possible lake influences on the bow echo as it passed over the GSL. Simulations were conducted first with a single $1000 \times 900\,\text{km}^2$ domain centred at 41.1 °N, 112.9 °W (the central GSL) with a 5 km grid spacing (Figure 2(a)) while the convective scheme was turned off. The 5 km model grid spacing was chosen because dominant circulations in midlatitude mesoscale convective systems (MCSs) have been shown to be depicted adequately near this resolution or higher (Weisman *et al.*, 1997). The simulations were initialized at 0600 UTC 21 April.

For the single-domain experiment, sensitivity tests were conducted using different MPSs in an attempt to reproduce the bow echo. These subsequent tests are referred to as Kessler, Lin, WSM 3, WSM 5, WSM 6, Goddard, Thompson and Morrison MPSs (references listed in Table 1). Other key physics schemes included the Yonsei University (YSU) planetary boundary layer (PBL) scheme (Hong *et al.*, 2006), CLM3.5 (Oleson *et al.*, 2008), and the Dudhia shortwave (Dudhia, 1989) and Rapid Radiative Transfer Model longwave (Mlawer *et al.*, 1997) radiation schemes. Six hourly NAM analyses were used for the initial and lateral boundary conditions. Physics schemes used in the NAM included the Betts–Miller–Janjić (BMJ; Betts, 1986; Betts and Miller, 1986, 1993; Janjić, 1994, 2003) cumulus parameterization, the Ferrier microphysics scheme (Ferrier *et al.*, 2002), and the Mellor–Yamada–Janjić (MYJ; Mellor and Yamada, 1982; Janjić, 2002) boundary layer parameterization. In later analysis, the NCEP Global Forecast System (GFS; Environmental Modeling Center, 2003) was used as initial and lateral boundary conditions.

Additional sets of experiments using forecasts initialized at 1800 UTC 21 April, that is, when the bow echo had just developed west of the GSL (Figure 1(a)), were also conducted. First, the impact of low-level moisture in the initial boundary conditions (to reflect observations more accurately) was examined with the 5 km grid spacing single-domain experiments. Second, simulations were conducted using three nested domains to examine the impact of enhancing resolution on the bow echo simulations; this aspect has been studied in the Central Plains but has not been explored in the Intermountain West. The three nested domains comprised the outermost domain (12 km grid spacing, horizontal dimension 130×120 grid points), the inner domain (4 km, 185×173), and the innermost domain (1 km, 202×181) and are shown in Figure 2(b). For the outermost domain, the BMJ cumulus parameterization was used. These three additional experiments used the same physics configurations as the single-domain simulations.

3. Results

3.1. Synoptic conditions

The bow echo of 21 April occurred during the rapid passage of a short-wave trough at the 700 hPa level across the Intermountain West. The short-wave trough was situated over the Sierra Nevada at 1200 UTC on 21 April (Figure 3(a)). At 300 hPa (not shown), the short-wave trough was located

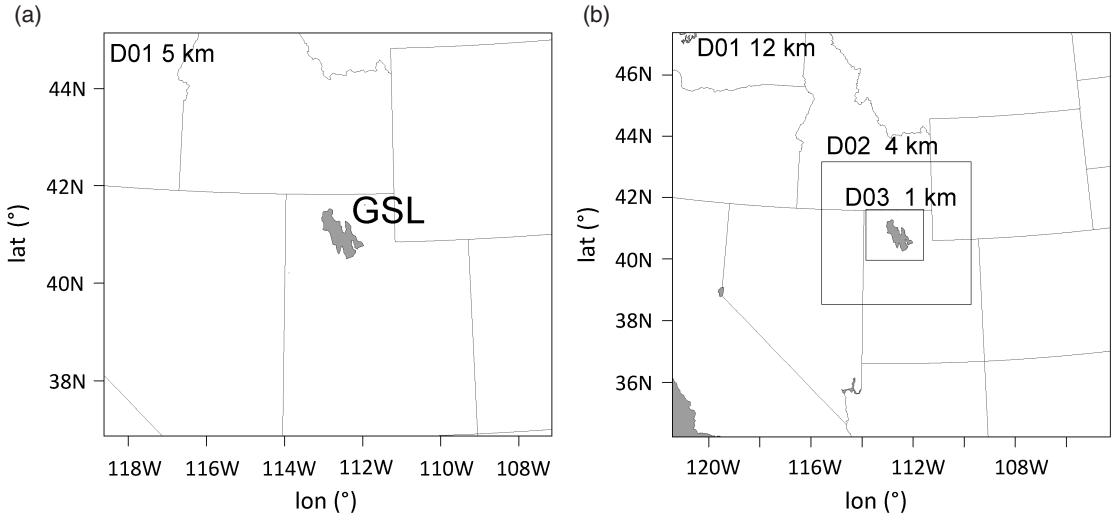

Figure 2. (a) The Advanced Research Weather Research and Forecasting model (ARW) single domain with 5 km grid spacing (D01) and (b) three nested domains with 12 km (D01), 4 km (D02), and 1 km (D03) grid spacing.

Table 1. MPS sensitivity tests of ARW simulations with 5 km grid spacing, and the corresponding RMSE and CC of domain averaged precipitation (as shown in Figure 5(a)) between observations and simulations with various MPSs. RMSE (−1 h) and CC (−1 h) represent a 1 h lag for the simulations compared to the observations.

MPSs	RMSE ($mm\,h^{-1}$)	CC	RMSE (−1 h; $mm\,h^{-1}$)	CC (−1 h)
Kessler scheme (Kessler, 1969)	0.17	0.47	0.10	0.87
Lin scheme (Lin *et al.*, 1983)	0.10	0.57	0.03	0.95
WSM 3-class simple ice scheme (Hong *et al.*, 2004)	0.14	0.27	0.08	0.73
WSM 5-class scheme (Hong *et al.*, 2004)	0.11	0.47	0.06	0.87
WSM 6-class graupel scheme (Hong and Lim, 2006)	0.11	0.48	0.05	0.91
Goddard scheme (Tao *et al.*, 1989)	0.16	0.37	0.09	0.87
Thompson scheme (Thompson *et al.*, 2008)	0.15	0.30	0.08	0.79
Morrison scheme (Morrison *et al.*, 2009)	0.19	0.45	0.14	0.79

in the West Coast (over the Cascade Mountains) indicating a strong baroclinic structure (because of its apparent westward tilt). The short-wave trough travelled across Nevada, Utah and half of Colorado by 0000 UTC on April 22 (Figure 3(b)). The larger-scale flow pattern resembles the type III synoptic regime documented by Maddox *et al.* (1980), which is conducive to flash floods in the Intermountain West. This so-called type-III regime consists of strong synoptic waves with cooler temperatures and strong winds aloft and can cause heavy rains over large areas. Harnack *et al.* (1998) also found that the 700 hPa circulation similar to the type-III pattern produces the majority of the warm-season rainfall in Utah. However, the short-wave trough around 21 April (Figures 3(a) and (b)) travelled at a speed faster than the typical cases documented by Harnack *et al.* (1998) and was associated with strong, cold northwesterly winds behind the cold front (Figures 3(c) and (d) surface maps).

Figure 4 illustrates the 700 hPa winds and relative vorticity (shading) from 0700 UTC 21 April through 2300 UTC based on RUC analyses. A subsynoptic-scale, cyclonic perturbation associated with the short-wave trough developed in the tri-state region between California, Nevada, and Oregon around 0700 UTC and then moved toward Idaho. However, this subsynoptic-scale perturbation moved more slowly than the larger scale background short-wave trough and dissipated after encountering the Rocky Mountains. At 1800 UTC, the bow echo had initiated to the east of this subsynoptic-scale perturbation located in the desert area west of the GSL (Figure 4(e), indicated with a black line).

Midtropospheric perturbations, such as the one associated with the 21 April bow echo, possess subsynoptic-scale features previously undocumented in climatological studies (Maddox *et al.*, 1980; Harnack *et al.*, 1998). These perturbations provide an essential vorticity source and uplift for storms along its leading edge, as has been observed in progressive MCSs across the Great Plains (Bosart and Sanders, 1981; Johns, 1984, 1993). In the Midwest during midsummer, when it is relatively dry under the prevailing northwesterly upper-level winds, up to 60% of rainfall and 80% of storm reports are linked to midtropospheric perturbations (Wang *et al.*, 2011). Wang *et al.* (2009a) pointed out that, in the Midwest, the performance of forecasting models on simulating midtropospheric perturbations is crucial in capturing the propagation and development of progressive MCSs including bow echoes; it will be shown in Section 3.4 that this is also the case for NAM simulations in the Intermountain West.

3.2. The simulations

3.2.1. Five kilometre grid spacing single-domain

Time series of hourly precipitation averaged over the GSL domain (Figure 5(a)) are shown in Figure 5(b). The simulations were conducted with eight different MPSs (Table 1); the Lin scheme appeared to generate an amount of precipitation that

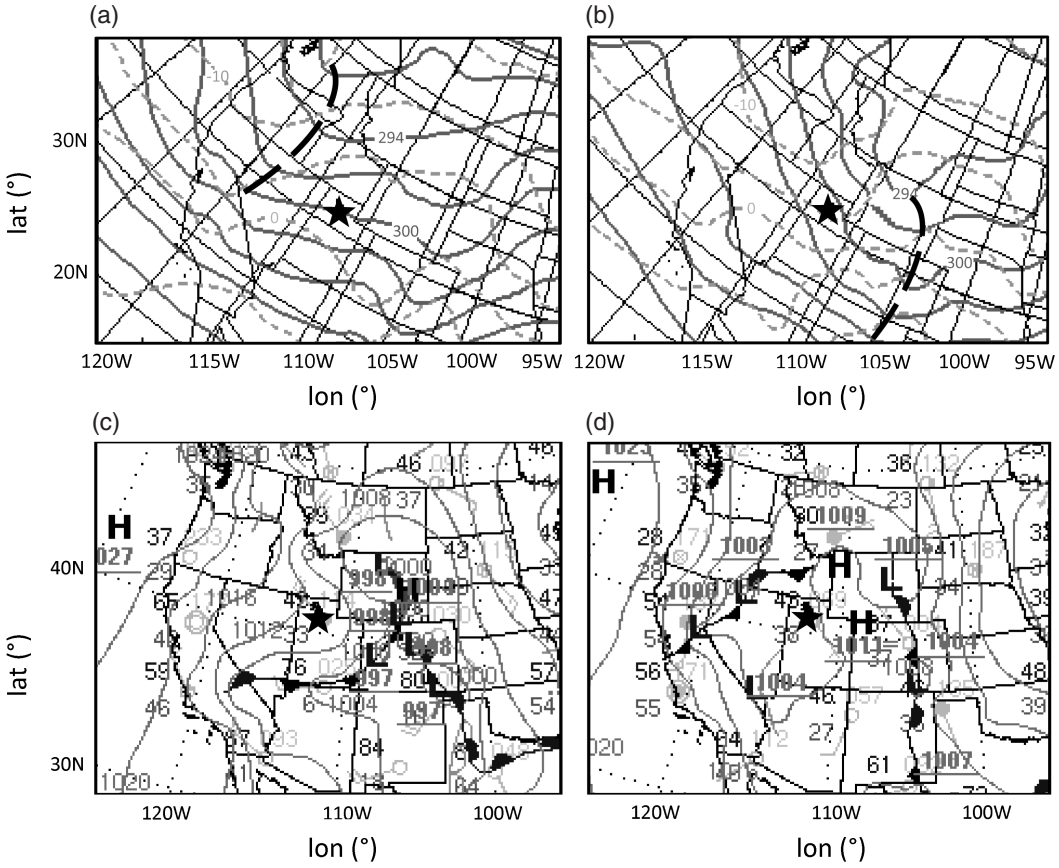

Figure 3. 700 hPa geopotential height and temperature, (a) at 1200 UTC 21 April 2011 and (b) at 0000 UTC 22 April 2011; surface charts (c) at 1200 UTC 21 April 2011 and (d) at 0000 UTC 22 April 2011. Star represents GSL area. Chart source: http://nomads.ncdc.noaa.gov/ncep/NCEP.

was closest to the observed. However, all these MPSs exhibited a delay in peak precipitation of 1–2 h compared with the observation, suggesting that the bias in storm propagation is not directly related to MPSs. Note that the domain over which the precipitation was averaged was cut off at the eastern edge of the GSL because ARW and NAM have a tendency to overpredict precipitation on the windward side of the Wasatch Range, a documented bias (Caldwell *et al.*, 2009; Wang *et al.*, 2009b) that may distort the depiction of storm precipitation. In order to quantify the differences between the precipitation simulations and the observations, their root mean square error (RMSE) and cross correlation (CC) were shown in Table 1, with the Lin scheme generating the lowest RMSE (0.03) and the highest CC (0.95) for precipitation. The RMSE and CC of different MPSs ranged from 0.10 to 0.19 and from 0.27 to 0.57, respectively, with the Lin MPS seemingly outperforming other MPSs. However, these simulations were generally unable to capture the spatial distribution of the precipitation, that is, the bow echo. The simulated vertical motion at 1900 UTC from different MPSs (not shown) indicated similar basic patterns over the GSL with different magnitude: updraft at the upper levels (above 4.7 km) and downdraft at the lower levels (below 4.7 km), with the Lin scheme generating the strongest upward motion over the lake. Using the Lin MPS, Figures 5(c) and (d) illustrate the observed and simulated precipitation patterns at 1800 UTC, 1900 UTC and 2000 UTC. While the simultaneous difference is substantial (Figure 5(c)), the difference with a 1 h lag appears smaller (i.e. comparing the 2000 UTC simulation with the 1900 UTC observation).

Next, the simulated reflectivity was examined, which was computed by adding the equivalent reflectivity factors for each simulated hydrometeor species (Koch *et al.*, 2005). As shown by the 6 h and 12 h NAM forecasts in Figures 6(a) (b), both failed to capture the bow echo development as observed (Figure 6(c)). It may be argued that the 6 h forecast did capture the northern arm of the storm, but the line structure is missing in the simulation. The inability of the NAM to depict the bow echo is not surprising, given its relatively coarse grid spacing, which makes it necessary to use a convective scheme. Indeed, simulations with eight different MPSs (Figures 6(d)–(k)) produced consistently line-convection structures, but with the wrong orientation (i.e. southwest–northeast) and widespread overprediction south of the GSL over desert areas. The simulations were not improved either, at the time when the bow echo reached its maximum intensity (~1900 UTC; not shown), while the southwest–northeast oriented bands grew even more intense and covered most of the domain as shown in Figure 6.

Next, by accounting for the temporal bias of about an hour (indicated in Figure 5(b)), the observed reflectivity valid at 1807 UTC (Figure 7(a)) with the simulated reflectivity at 1915 UTC (initialized at 1800 UTC 21 April) were compared using the Lin MPS. As is shown in Figure 7(b), it appears that the bow echo in its initial stage is depicted reasonably with a consistent maximum reflectivity to the west of the GSL (regardless of the delay). Likewise, when comparing the simulated bow echo pattern at 2000 UTC (Figure 7(f)) with the 1854 UTC observation (Figure 7(e)), it is clear that the ARW produces the observed pattern reasonably even though the simulated reflectivity appears discontinuous and underestimated.

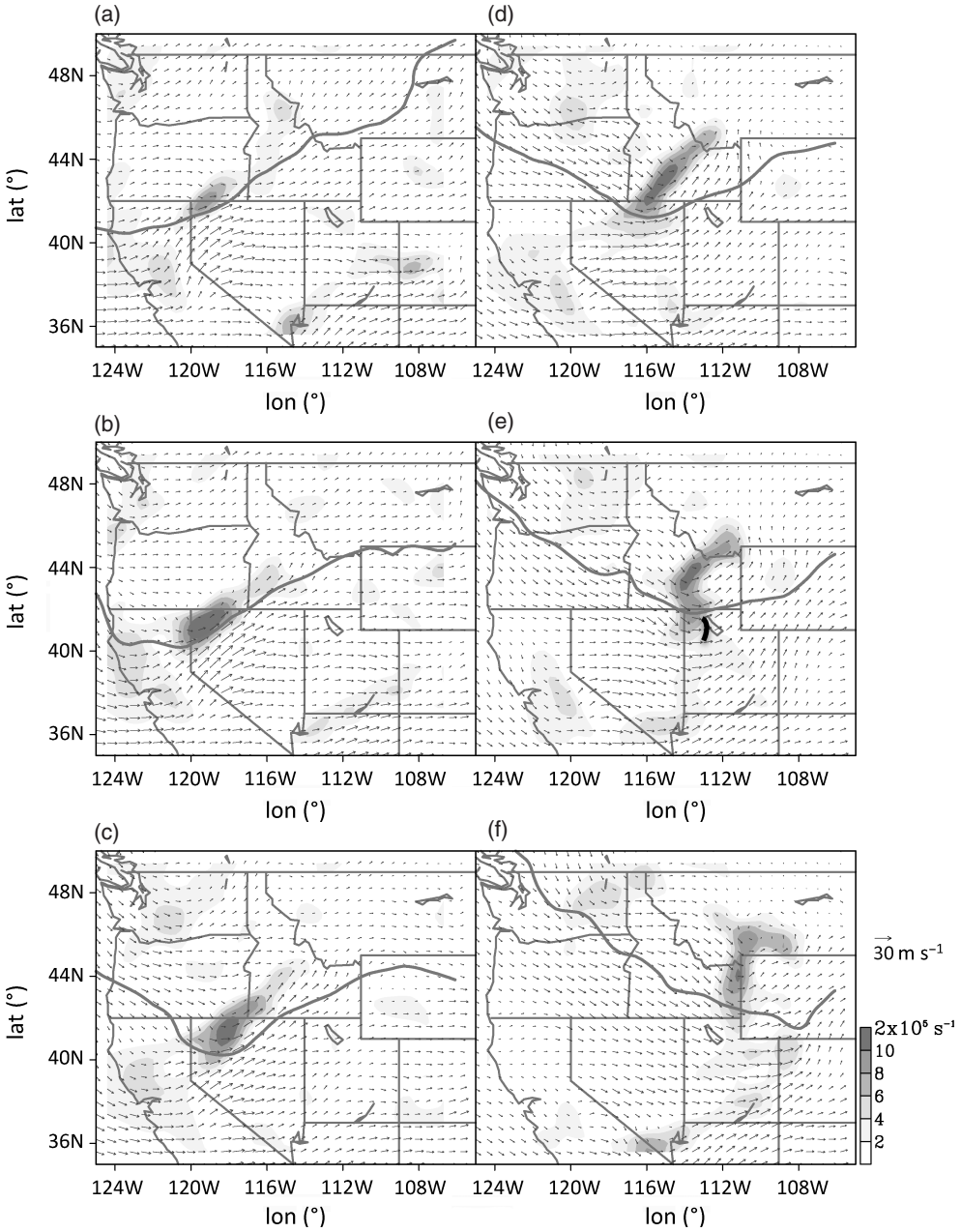

Figure 4. 700 hPa wind and relative vorticity (shaded) on 21 April 2011, (a) 0700 UTC, (b)1000 UTC, (c)1300 UTC, (d) 1600 UTC, (e) 1800 UTC, (f) 2300 UTC. Grey line represents geopotential height of 2975 gpm, black line in (e) represents bow echo.

3.2.2. Enhanced moisture and nested domains

By comparing the mixing ratio (q) of the Salt Lake City sounding (KSLC) at 1200 UTC 21 April with model simulations, it was found that the simulated middle-to-lower troposphere was too dry, with a 13–22% deficit in q throughout the layer of 850–600 hPa (results not shown). It was noted by Wang *et al.* (2009a) that NAM has a dry bias in warm-season climatology. Thus, in the next experiment q was increased artificially by 50% over the desert area west of the GSL (114.3–112.5 °W, 39.5–41.3 °N). This exaggerated percent increase in q was to highlight the sensitivity of bow echo simulations to the moisture content. As shown in Figures 7(c) and (g), the simulated reflectivity intensified and was closer to the observation after the moisture increase, but the simulations still did not produce any apparent bow echo structure. On the other hand, the 1 km inner domain of the nested simulations (Figure 7(d)) produced reflectivity as intense as the enhanced-moisture experiment (Figure 7(c)), even though moisture in the 1 km simulation was not increased. Noteworthy is the 2000 UTC reflectivity of the 1 km simulation (Figure 7(h)), which reveals a well-defined bow echo pattern east of the GSL. These finer-scale structure and more realistic features depicted in the 1 km versus the 5 km simulations are consistent with the comparisons made between 1 and 4 km grid spacing ARW simulations for the Great Plains (see Clark *et al.*, 2012 and references therein).

3.3. Sensitivity of lake simulations

Because of the difference in moisture and temperature between the land and lake surface layers during different seasons, convective systems can be either enhanced or weakened when

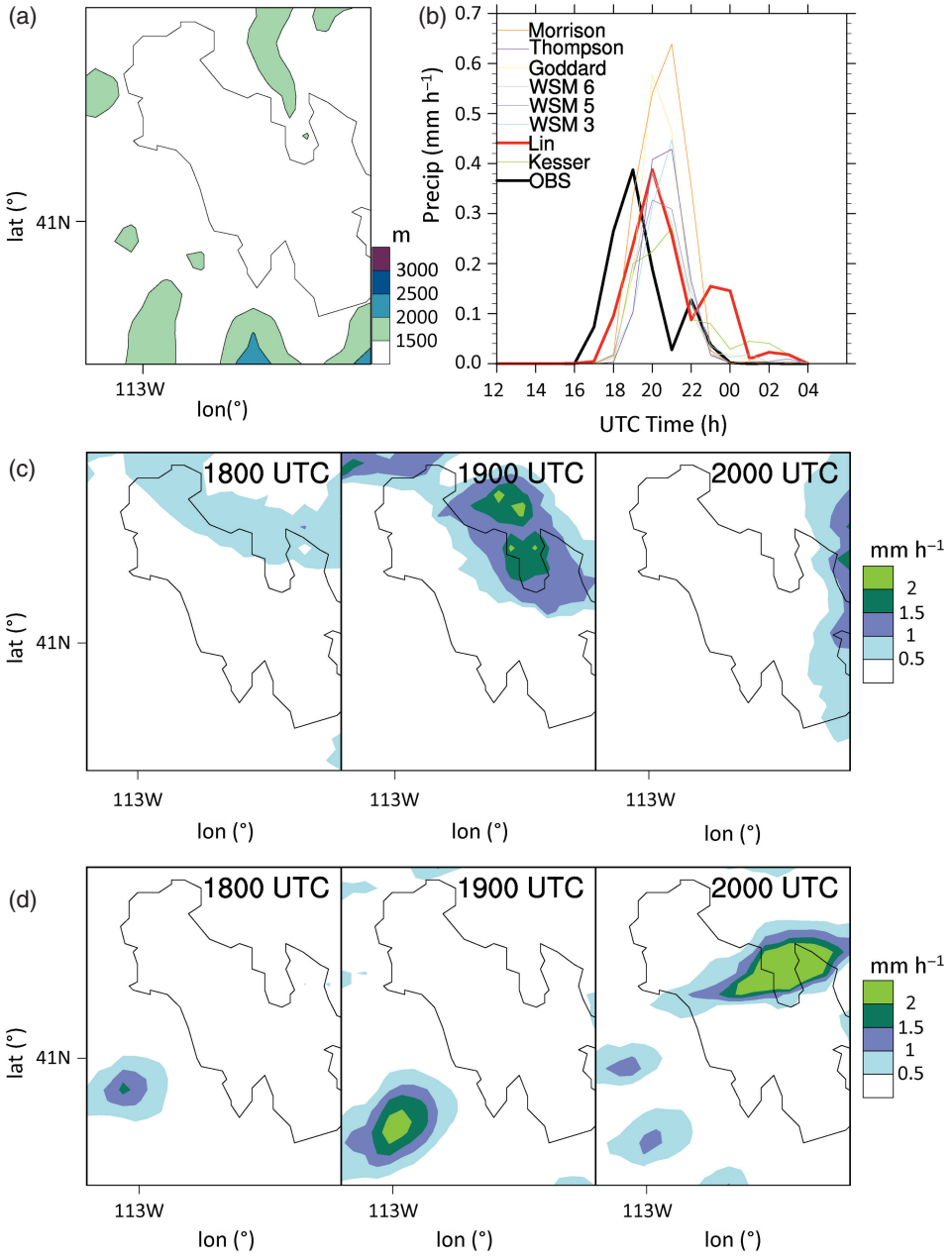

Figure 5. (a) Terrain map around Great Salt Lake (GSL), (b) time series of hourly precipitation (mm h^{-1}) averaged over the GSL domain (i.e. the domain as (a)) observation compared against simulations with different microphyics schemes (MPSs), (c) and (d) are hourly spatial distributions of observed and Lin MPS-simulated precipitation (mm h^{-1}) during 1800–2000 UTC on 21 April 2011, respectively.

they pass over large lakes such as the GSL. During the cold season, higher lake temperatures may enhance moisture and instability for convection, but convective systems emanating directly from lake effects occur rarely (such as thundersnow); this has been the case for the GSL (Market *et al.*, 2002). In the warm season, lakes have mixed impacts on convective systems depending on the environmental conditions of lake breezes and low-level wind shear, as is the case for the Great Lakes (Kristovich *et al.*, 2003). As far as is known, the GSL has not been documented to have any systematic effect on springtime convective storms passing over it.

The lake surface temperature using the MODIS daily product (MYD11C1) was first examined. Owing to cloud cover on 21 April, the April 20 night time measurement was used for the lake surface temperature. As shown in Figure 8(a), the GSL surface temperature was at the 2–6 °C range, given that lake temperature does not change much within one day. By computing the temperature difference between the surface on 20 April 2011 using night time MODIS data and the 700 hPa level at 1800 UTC on 21 April using RUC data, a 6–10 °C temperature difference (or lapse rate) was observed between the GSL (elevation ~1300 m) and the 700 hPa level (Figure 8(b)). Such a lapse rate is almost dry-adiabatic and therefore presents a potential for lake-enhanced convection (Steenburgh *et al.*, 2000; Zhao *et al.*, 2012). Thus, the impact of the GSL on the rather rapid development of the bow echo was examined next.

On the basis of the sensitivity simulations shown in Figure 5(b), six of the better-performing MPSs (of the original eight) were chose to repeat the simulations *without* the GSL

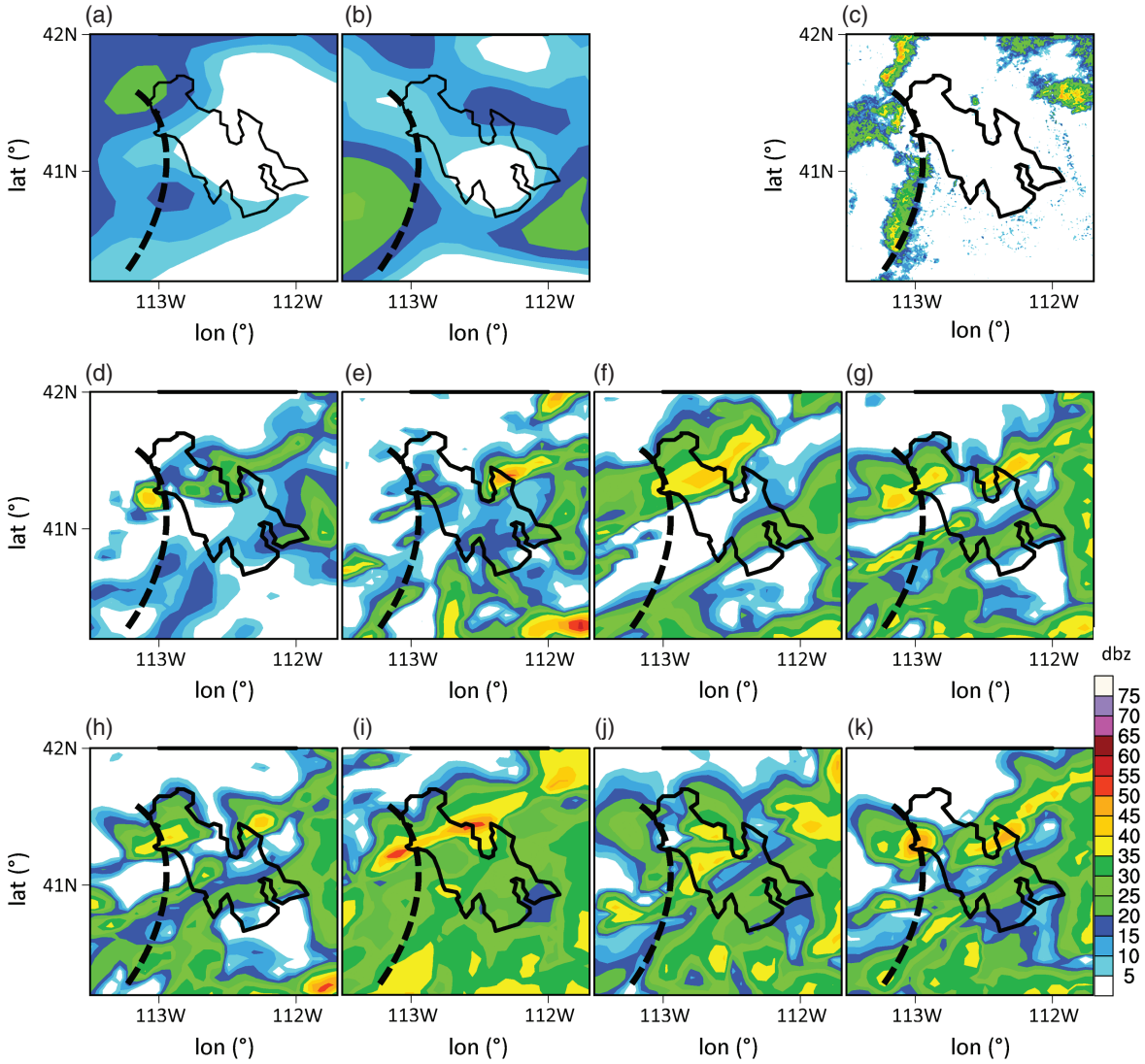

Figure 6. Comparison of composite reflectivity (dbz) over the Great Salt Lake (GSL) among observations, North American Mesoscale (NAM) forecasts, and the Advanced Research Weather Research and Forecasting model (ARW) simulations around 1800 UTC 21 April 2011, (a) NAM 6 h forecast from 1200 UTC and (b) NAM 12 h forecast from 0600 UTC 21 April 2011, respectively, (c) observation at 1807 UTC, simulated composite reflectivity with microphysics schemes (MPSs) of (d) Kessler, (e) Lin, (f) WSM 3, (g) WSM 5, (h) WSM 6, (i) Goddard, (j) Thompson, and (k) Morrison, respectively. Black dashed line indicates bow echo.

(i.e. no-lake experiment), which involved substituting the surrounding land-use type of shrubland for the lake. The storm precipitation was integrated for 1600–0000 UTC averaged within the domain as in Figure 5(a). The results in Figure 9, however, do not reveal any consistent difference between the no-lake and control experiments, that is, precipitation is higher in some no-lake experiments of certain MPSs (e.g. WSM 6 and Thompson) but lower in other MPSs (e.g. WSM 5 and Goddard). The magnitude of these precipitation differences is within 5% and considered insignificant. It appears that the inclusion of the GSL did not impact the simulation of the MCS. A possible factor leading to this lack of GSL effect is the rather cold lake surface (2–6 °C) that might increase stability in the lower troposphere.

3.4. Dynamical implications

Examining numerical forecasts of summertime subsynoptic perturbations in the Upper Midwest, Wang *et al.* (2009a) found that NAM consistently underestimated the propagation speed of the perturbations, leading to a displacement in the precipitation patterns associated with the MCS. Such a propagation speed bias is similar to the delay of the simulated bow echo as shown in Figure 5. By using the 725 hPa geopotential height and relative vorticity maximum at 1800 UTC 21 April as the reference point, the position of the simulated midtropospheric perturbation was compared against that observed (Figure 10(a)). The vorticity centres (i.e. trough lines) of the NAM 6 h forecast and two NAM-forced ARW simulations (one at the same time and the other earlier at 0600 UTC April 20) all fall behind the observed one, suggesting a speed bias. The bias in the 1800 UTC simulation (green line) is alarming because it suggests an initial error of the ARW that is likely to grow over the integration, as is evidenced by the more pronounced speed bias in the 0600 UTC simulation (blue line).

Meanwhile, when forced by GFS as initial boundary conditions, the simulated vorticity centres (orange and purple lines) were very close to the observed, suggesting that the aforementioned speed bias may only result from the NAM.

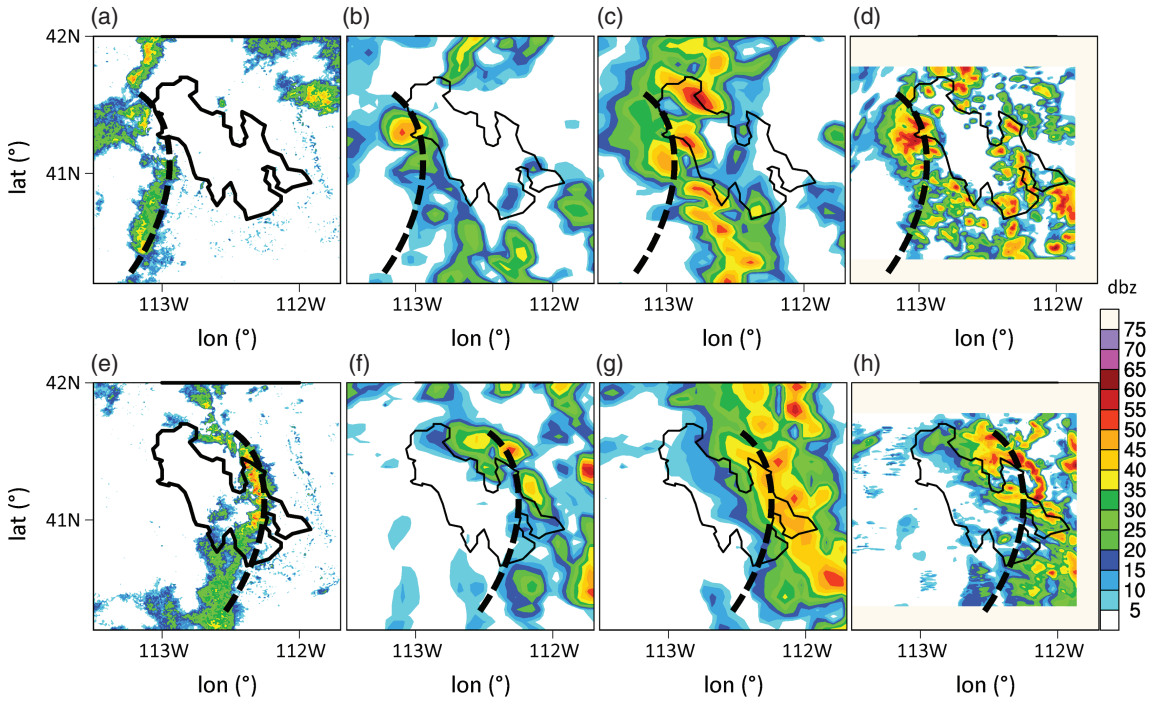

Figure 7. Comparison between observations and the Advanced Research Weather Research and Forecasting model (ARW) simulations initialized at 1800 UTC 21 April, (a) observation at 1807 UTC, (b) simulated composite reflectivity (dbz) over the Great Salt Lake (GSL) with Lin microphysics site (MPS) at 1915 UTC (original), (c) simulated composite reflectivity at 1915 UTC by enhancing moisture within the whole model layer with Lin MPS, (d) simulated composite reflectivity of the innermost domain at 1915 UTC using three nested simulation with Lin MPS, (e) observation at 1854 UTC, (f)–(h) the simulated results are the same as those of first row but at 2000 UTC. Black dashed line indicates bow echo.

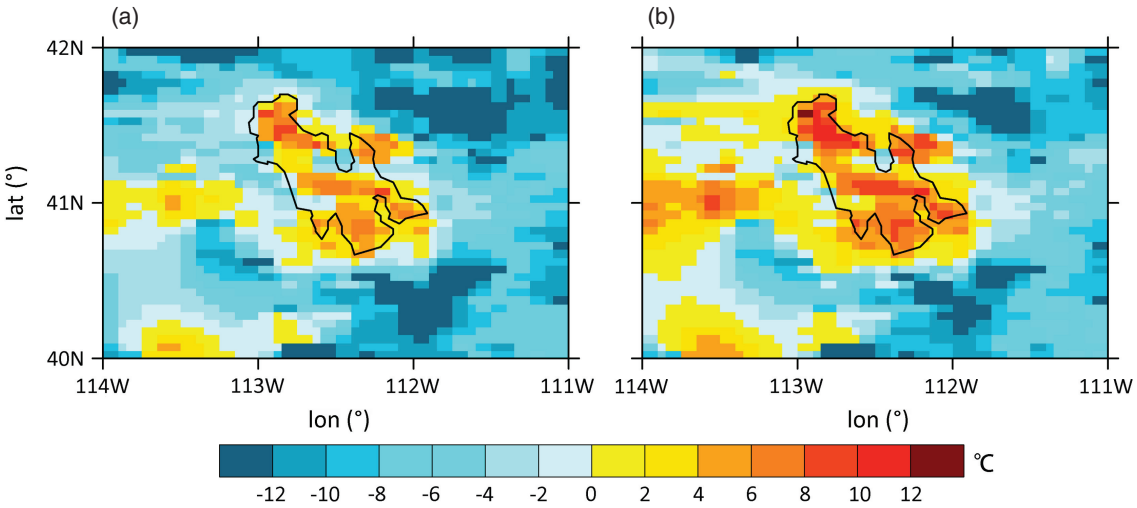

Figure 8. (a) Moderate Resolution Imaging Spectroradiometer (MODIS) lake surface temperature of night time on 20 April 2011 and (b) temperature difference (lake surface temperature minus 700 hPa temperature) between the MODIS lake surface temperature of night time on 20 April 2011 and 700 hPa temperature of the Rapid Update Cycle model (RUC) at 1800 UTC on 21 April 2011.

Nevertheless, precipitation of the GFS-forced simulation, conducted with the single domain (Figure 2(a)) at 5 km grid spacing, was underpredicted severely (Figure 11 grey dashed line) although the timing is apparently improved in comparison with Figure 5(b), here for brevity only the simulation that the Lin MPS used is presented. On the contrary, precipitation simulated from the 1 km GFS-forced simulation was overestimated considerably (Figure 11 grey solid line), but revealed a further improvement in the timing. Nevertheless, examination of the simulated reflectivity pattern (not shown) indicated that neither the 5 km nor the 1 km simulation reproduced the bow echo, although the 1 km run generated a rainband that is more consistent with the observation than the 5 km run and without delay.

It is prudent to examine further the speed bias associated with NAM, as it is the primary regional forecasting model in operation. Thus, three NAM forecasts (f06, f12, and f24) were analysed in comparison with the analysis (f00). On the basis of the approach explained next, three midtropospheric perturbation cases similar to that on 21 April 2011 were selected

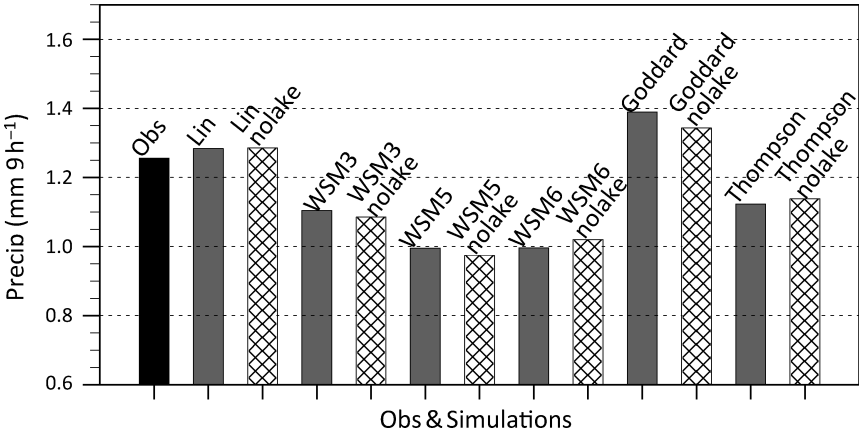

Figure 9. Comparison of domain averaged (i.e. the domain as Figure 5(a)) precipitation (mm 9 h^{-1}) integrated for 1600–0000 UTC between observation (black) and the Advanced Research Weather Research and Forecasting model (ARW) simulations with different microphysics sites. Grey and hatched bars represent runs with and without Great Salt Lake (GSL), respectively.

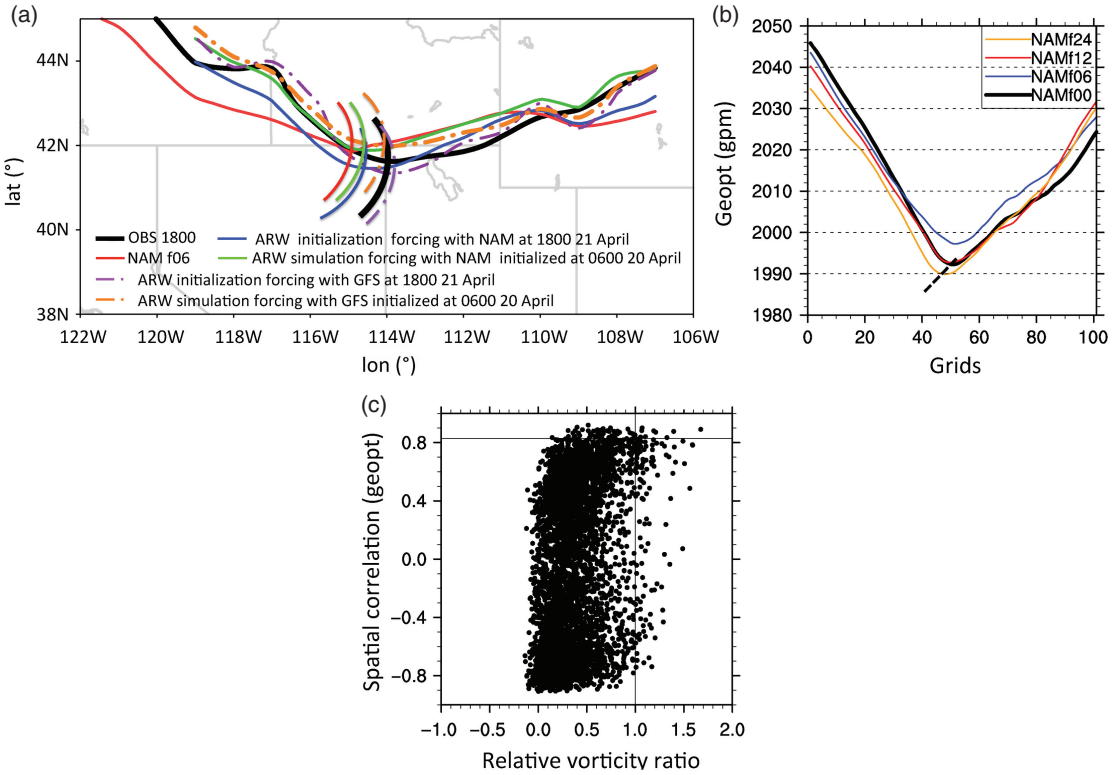

Figure 10. (a) Comparison of 725 hPa geopotential height of 2700 gpm among different data (i.e. Rapid Update Cycle model (RUC), North American Mesoscale model (NAM) forecast, Advanced Research Weather Research and Forecasting model (ARW) simulation, and ARW initialization) at 1800 UTC 21 April 2011: black line, red line, blue line, green line, purple line dot, and orange line dot represent the geopotential height of observations (i.e. RUC), NAM f06, ARW initialization forced with NAM at 1800 UTC, ARW simulation forced with NAM initialized at 0600 UTC21 April 2011, ARW initialization forced with GFS, and ARW simulation forced with GFS initialized at 0600 UTC21 April 2011, respectively, (b) composite geopotential height of three cases (details in text) similar with the case of 1800 UTC 21 April 2011 based on the NAM 00, 06, 12, and 24 h forecasts, (c) 725 hPa relative vorticity ratio *versus* spatial correlation of geopotential height between bow echo (i.e. 1800 UTC 21 April 2011) and the other 3 h interval of NARR data (1991–2010).

for analysis: 20070418 1800 UTC, 20070423 0900 UTC, and 20090415 2100 UTC (i.e. the NAM archive only dates back to 2007). A composite approach was adopted by aligning the 725 hPa trough (vorticity centre) location of each perturbation based on f00 and then averaging for f06, f12, and f24 with geopotential height. The composite f00 geopotential height contour was averaged between 40 and 41.5 °N, centred at the point of the lowest geopotential height and expanded horizontally for 50 grid points (Figure 10(b) black line). It was then overlaid with the same grids of forecast geopotential height contours in colour. There is a discernable position shift (or delay) in the trough location at f12 and further at f24 compared with f00. This result suggests that the speed bias of midtropospheric perturbations in the NAM, similar to that documented in Wang *et al.* (2009a), is also present in the Intermountain West.

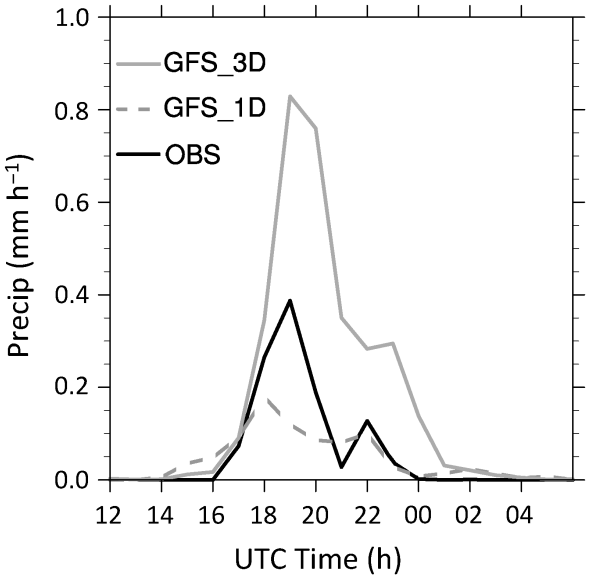

Figure 11. Time series of domain averaged (i.e. the domain as Figure 5(a)) precipitation (mm h^{-1}). Black line represents observation, grey dashed and grey solid lines represent precipitation of Global Forecast System (GFS) forced simulations with single domain (Figure 2(a)) and the innermost three nested domains (Figure 2(b)), initialized at 0600 UTC 21 April 2011, respectively.

Given the close correspondence between bow echoes and subsynoptic perturbations in the midwestern United States (Trier *et al.*, 2006; Wang *et al.*, 2011), it also appears necessary to examine the frequency of which strong midtropospheric perturbations occur in the western United States. Thus, the frequency of perturbations was first examined at the similar scale and amplitude as the 21 April 2011 case (cf. Figure 4). However, because neither the NAM nor RUC provides a long enough archive of data and because both models have undergone several upgrades over the years, the NARR 3 h data was used to trace the occurrence of similar perturbations in April from 1991 to 2010. Within the domain 125–105 °W and 35–45 °N (Figure 10(a)), the 725 hPa geopotential height 'eddy' (with the domain zonal mean removed) was compared against the situation on 1800 UTC 21 April 2011, based on the analysis of spatial correlation for each 3 h interval. Next, the maximum of the 725 hPa relative vorticity was averaged over the GSL vicinity domain of 116–112 °W, 40–44 °N; comparing this value with that of 1800 UTC 21 April obtained a ratio that represents the vorticity intensity relative to the 21 April case. The spatial correlation of geopotential height and the vorticity ratio are shown as a scatter diagram in Figure 10(c).

On the basis of the threshold of spatial correlation greater than 0.8 (an arbitrary value) and vorticity ratio greater than 1, only seven such perturbations were found: 1 April 1999 1500 UTC, 20 April 2005 0600 UTC, 20 April 2005 2100 UTC, 6 April 2006 0600 UTC, 18 April 2007 1800 UTC, 23 April 2007 0900 UTC, 1 April 2009 0000 UTC, and 15 April 2009 2100 UTC), three of which are the cases used for Figure 10(b). It appears that strong perturbations as intense as the case of 21 April 2011 have occurred more frequently during recent years (after 2005), although none of those perturbations generated a bow echo. This result highlights the need for further research in assessing extreme weather under the warming climate of this region (Gillies *et al.*, 2012).

4. Conclusions

In April 2011, a rare bow echo occurred in the desert region of the Salt Flats and the Great Salt Lake (GSL) in Utah. This bow echo produced high, damaging winds in residential areas along the Wasatch Range east of the GSL. The operational North American Mesoscale (NAM) model, developed from the WRF non-hydrostatic model, failed to forecast this event even when initialized just 6 h earlier. In order to assess the possibility of this type of extreme weather occurring in the future under regional climate warming and increasing storm intensity (Gillies *et al.*, 2012), a model evaluation study was carried out for this bow echo event using the Advanced Research Weather Research and Forecasting (WRF) model (ARW). The model's performance in simulating this bow echo and associated weather system is documented here. This provides important information for ARW to be used in subsequent regional downscaling studies over this region, including the study initiated by this team (Jin *et al.*, 2011) as well as by others (Shem *et al.*, 2012; Yoon *et al.*, 2012).

The results of the ARW simulations for this springtime bow echo are summarized as follows:

(1) Finer resolution is necessary to produce bow echoes: comparing the 5 and 1 km simulations, the 1 km run produced the fine-scale convective features of line convection that are more realistic than those produced by the 5 km run. This result is in agreement with many previous studies that focused on mesoscale convective systems simulations in the central and southern United States.
(2) Storm formation is sensitive to moisture content: the atmospheric moisture content, which exhibits a dry bias in NAM over the arid GSL area, affects the bow echo simulation at the 5 km grid spacing (but not at 1 km grid). Enhancing the moisture content to match better the reality subsequently intensified and improved the precipitation simulation at this grid spacing, but did not improve the simulation of bow echo formation (which only appeared in the 1 km run).
(3) Lake effect is minimal: although this bow echo appeared to have intensified rapidly over the GSL, comparison of no-lake simulation with control simulation suggested that the lake appears to suppress convection because of increased stability provided by the cool lake surface. However, this result is not consistent among the simulations using different microphysics schemes, and the precipitation differences were small.
(4) Important forcing source of the midtropospheric perturbation: while the NAM exhibited a bias in the propagation of the perturbation that accompanied the bow echo, ARW inherited this speed bias causing the displacement of the perturbation. This in turn resulted in the 1–2 h 'delay' of storm formation over the GSL. A simple remedy for this error is to force ARW with the NCEP Global Forecast System (GFS), a global model, rather than with a regional model such as the NAM. This finding highlights a potential risk of regional climate downscaling from regional model outputs, an approach that has been used increasingly for the Intermountain West (Gutmann *et al.*, 2012; Salzmann and Mearns, 2012).

Finally, as the bow echo of 21 April 2011 and the associated midtropospheric perturbation is uncommon in the rugged, semiarid Intermountain West, there is a greater need to assess the extent of which similar bow echoes could occur in the

future under the warming climate. Given the above analysis, there lies at least two challenges for modelling weather and climate in this region: (a) in terms of forecasting, the bias of NAM in simulating the propagation of bow echo-producing midtropospheric perturbations is likely to be a significant obstacle; (b) in terms of regional climate downscaling, any future climate projection of extreme convective storms in this region should apply adequate model resolution and accurate moisture content, as well as adopt the use of global models as initial boundary conditions.

Acknowledgements

Assistance of processing radar images by Chris Karstens is highly appreciated. This work was supported by the Strategic Priority Research Programme (B) of the Chinese Academy of Sciences (XDB03030300), National Natural Science of foundation of China (41130961), the Utah Agricultural Experiment Station, the NOAA MAPP NA090AR4310195 grant and NASA Grant NNX13AC37G.

References

Atkins NT, St. Laurent M. 2009a. Bow echo mesovortices. Part I: processes that influence their damaging potential. *Mon. Weather Rev.* **137**: 1497–1513.

Atkins NT, St. Laurent M. 2009b. Bow echo mesovortices. Part II: their genesis. *Mon. Weather Rev.* **137**: 1514–1532.

Baldwin ME, Mitchell KE. 1997. The NCEP hourly multi-sensor US precipitation analysis for operations and GCIP research. In *13th Conference on Hydrology, Long Beach, CA*. American Meteorological Society: Boston, MA.

Benjamin SG, Dévényi D, Weygandt SS, Brundage KJ, Brown JM, Grell GA, Kim D, Schwartz BE, Smirnova TG, Smith TL. 2004a. An hourly assimilation-forecast cycle: the RUC. *Mon. Weather Rev.* **132**: 495–518.

Benjamin SG, Grell GA, Brown JM, Smirnova TG, Bleck R. 2004b. Mesoscale weather prediction with the RUC hybrid isentropic-terrain-following coordinate model. *Mon. Weather Rev.* **132**: 473–494.

Betts A, Miller M. 1986. A new convective adjustment scheme. Part II: single column tests using GATE wave, BOMEX, ATEX and arctic air-mass data sets. *Q. J. R. Meteorol. Soc.* **112**: 693–709.

Betts AK, Miller M. 1993. The Betts-Miller scheme. In *The Representation of Cumulus Convection in Numerical Models of the Atmosphere*, Emanuel KA, Raymond DJ (eds). American Meteorological Society: Boston, MA; 107–121.

Betts AK. 1986. A new convective adjustment scheme. Part I: observational and theoretical basis. *Q. J. R. Meteorol. Soc.* **112**: 677–691.

Bosart LF, Sanders F. 1981. The Johnstown flood of July 1977: a long-lived convective system. *J. Atmos. Sci.* **38**: 1616–1642.

Burke PC, Schultz DM. 2004. A 4-yr climatology of cold-season bow echoes over the continental United States. *Weather Forecast.* **19**: 1061–1074.

Businger S, Birchard T Jr, Kodama K, Jendrowski PA, Wang J-J. 1998. A bow echo and severe weather associated with a Kona low in Hawaii. *Weather Forecast.* **13**: 576–591.

Caldwell P, Chin H-NS, Bader DC, Bala G. 2009. Evaluation of a WRF dynamical downscaling simulation over California. *Clim. Change* **95**: 499–521.

Clark AJ, Weiss SJ, Kain JS, Jirak IL, Coniglio M, Melick CJ, Siewert C, Sobash RA, Marsh PT, Dean AR. 2012. An overview of the 2010 hazardous weather testbed experimental forecast program spring experiment. *Bull. Am. Meteorol. Soc.* **93**: 55–74.

Crosman ET, Horel JD. 2009. MODIS-derived surface temperature of the Great Salt Lake. *Remote Sens. Environ.* **113**: 73–81.

Crum TD, Alberty RL, Burgess DW. 1993. Recording, archiving, and using WSR-88D data. *Bull. Am. Meteorol. Soc.* **74**: 645–653.

Dudhia J. 1989. Numerical study of convection observed during the winter monsoon experiment using a mesoscale two-dimensional model. *J. Atmos. Sci.* **46**: 3077–3107.

Environmental Modeling Center. 2003. '*The GFS Atmospheric Model*.' NCEP Office Note 442, Global Climate and Weather Modeling Branch, EMC, Camp Springs, MD.

Ferrier B, Jin Y, Lin Y, Black T, Rogers E, DiMego G. 2002. Implementation of a new grid-scale cloud and precipitation scheme in the NCEP Eta model. In *15th Conference on Numerical Weather Prediction, San Antonio, Tex*. American Meteorological Society: Boston, MA.

Fujita TT. 1978. *Manual of downburst identification for project Nimrod*. Satellite and Mesometeorology Research Paper 156. Dept. of Geophysical Sciences, University of Chicago, 104 pp.

Funk TW, DeWald VL, Lin YJ. 1998. A detailed WSR-88D Doppler radar evaluation of a damaging bow-echo event on 14 May 1995 over north-central Kentucky. In *19th Conference on Severe Local Storms, Minneapolis, MN*. American Meteorological Society: Boston, MA.

Gillies RR, Wang S-Y, Booth MR. 2012. Observational and synoptic analyses of the winter precipitation regime change over Utah. *J. Clim.* **25**: 4679–4698.

Gutmann ED, Rasmussen RM, Liu C, Ikeda K, Gochis DJ, Clark MP, Dudhia J, Thompson G. 2012. A comparison of statistical and dynamical downscaling of winter precipitation over complex terrain. *J. Clim.* **25**: 262–281.

Harnack RP, Jensen DT, Cermak JR III. 1998. Investigation of upper-air conditions occurring with heavy summer rain in Utah. *Int. J. Climatol.* **18**: 701–723.

Hong SY, Dudhia J, Chen SH. 2004. A revised approach to ice microphysical processes for the bulk parameterization of clouds and precipitation. *Mon. Weather Rev.* **132**: 103–120.

Hong SY, Lim JOJ. 2006. The WRF single-moment 6-class microphysics scheme (WSM 6). *J. Korean Meteor. Soc.* **42**: 129–151.

Hong SY, Noh Y, Dudhia J. 2006. A new vertical diffusion package with an explicit treatment of entrainment processes. *Mon. Weather Rev.* **134**: 2318–2341.

James RP, Markowski PM, Fritsch JM. 2006. Bow echo sensitivity to ambient moisture and cold pool strength. *Mon. Weather Rev.* **134**: 950–964.

Janjić ZI. 2003. A nonhydrostatic model based on a new approach. *Meteorol. Atmos. Phys.* **82**: 271–285.

Janjić ZI. 1994. The step-mountain eta coordinate model: further developments of the convection, viscous sublayer, and turbulence closure schemes. *Mon. Weather Rev.* **122**: 927–945.

Janjić ZI. 2002. *Nonsingular implementation of the Mellor–Yamada level 2 .5 scheme in the NCEP Meso model*. NCEP office note, **437**: 61.

Jin J, Miller NL, Schlegel N. 2010. Sensitivity study of four land surface schemes in the WRF model. *Adv. Meteorol.* **2010**: 167436, DOI: 10.1155/2010/167436.

Jin J, Wang SY, Gillies RR. 2011. An improved dynamical downscaling for the western United States. In *Climate Change/Book 2*, Pignatello R (ed). InTech: Vienna, DOI: 979-953-307-277-6.

Johns RH. 1984. A synoptic climatology of northwest-flow severe weather outbreaks. Part II: meteorological parameters and synoptic patterns. *Mon. Weather Rev.* **112**: 449–464.

Johns RH. 1993. Meteorological conditions associated with bow echo development in convective storms. *Weather Forecast.* **8**: 294–299.

Kessler E. 1969. *On the Distribution and Continuity of Water Substance in Atmospheric Circulation*, Meteor. Monogr., Vol. 32. American Meteorological Society: Boston, MA; 84.

Klimowski BA, Hjelmfelt MR, Bunkers MJ. 2004. Radar observations of the early evolution of bow echoes. *Weather Forecast.* **19**: 727–734.

Koch SE, Ferrier B, Stoelinga MT, Szoke E, Weiss SJ, Kain JS. 2005. The use of simulated radar reflectivity fields in the diagnosis of mesoscale phenomena from high-resolution WRF model forecasts. In *11th Conference on Mesoscale Processes, Albuquerque, NM*. American Meteorological Society: Boston, MA http://ams.confex.com/ams/32Rad11Meso/techprogram/paper_97032.htm.

Kristovich DAR, LaPlante R, Laird NF, Kubina WT. 2003. Are thunderstorms that form along lake breezes more intense?. In *Midwest Severe and Hazardous Weather Conference, Central Illinois*. American Meteorological Society: Boston, MA.

Lin YL, Farley RD, Orville HD. 1983. Bulk parameterization of the snow field in a cloud model. *J. Clim. Appl. Meteorol.* **22**: 1065–1092.

Maddox RA, Canova F, Hoxit LR. 1980. Meteorological characteristics of flash flood events over the western United States. *Mon. Weather Rev.* **108**: 1866–1877.

Market PS, Halcomb CE, Ebert RL. 2002. A climatology of thundersnow events over the contiguous United States. *Weather Forecast.* **17**: 1290–1295.

Mellor GL, Yamada T. 1982. Development of a turbulence closure model for geophysical fluid problems. *Rev. Geophys.* **20**: 851–875.

Mesinger F, DiMego G, Kalnay E, Mitchell K, Shafran PC, Ebisuzaki W, Jovic D, Woollen J, Rogers E, Berbery EH. 2006. North American regional reanalysis. *Bull. Am. Meteorol. Soc.* **87**: 343–360.

Mlawer EJ, Taubman SJ, Brown PD, Iacono MJ, Clough SA. 1997. Radiative transfer for inhomogeneous atmospheres: RRTM, a validated correlated-k model for the longwave. *J. Geophys. Res.* **102**: 16663–16682.

Morrison H, Thompson G, Tatarskii V. 2009. Impact of cloud microphysics on the development of trailing stratiform precipitation in a simulated squall line: comparison of one-and two-moment schemes. *Mon. Weather Rev.* **137**: 991–1007.

Oleson K, Niu GY, Yang ZL, Lawrence D, Thornton P, Lawrence P, Stöckli R, Dickinson R, Bonan G, Levis S. 2008. Improvements to the Community Land Model and their impact on the hydrological cycle. *J. Geophys. Res.* **113**: G01021.

Salzmann N, Mearns LO. 2012. Assessing the performance of multiple regional climate model simulations for seasonal mountain snow in the Upper Colorado River Basin. *J. Hydrometeorol.* **13**: 539–556.

Schoen JM, Ashley WS. 2011. A climatology of fatal convective wind events by storm type. *Weather Forecast.* **26**: 109–121.

Shafer JC, Steenburgh WJ. 2008. Climatology of strong Intermountain cold fronts. *Mon. Weather Rev.* **136**: 784–807.

Shamarock W, Klemp J, Dudhia J, Gill D, Barker D, Duda M, Huang X, Wang W, Powers J. 2008. *A description of the advanced research WRF version 3*. Technical note TN–475+STR. NCAR: Boulder, Colorado, USA.

Shem WO, Mote T, Shepherd J. 2012. Validation of NARCCAP temperature data for some forest sites in the southeast United States. *Atmosph. Sci. Lett.* **13**: 275–282.

Steenburgh WJ, Halvorson SF, Onton DJ. 2000. Climatology of lake-effect snowstorms of the Great Salt Lake. *Mon. Weather Rev.* **128**: 709–727.

Tao W-K, Simpson J, McCumber M. 1989. An ice-water saturation adjustment. *Mon. Weather Rev.* **117**: 231–235.

Thompson G, Field PR, Rasmussen RM, Hall WD. 2008. Explicit forecasts of winter precipitation using an improved bulk microphysics scheme. Part II: implementation of a new snow parameterization. *Mon. Weather Rev.* **136**: 5095–5115.

Trapp RJ, Weisman ML. 2003. Low-level mesovortices within squall lines and bow echoes. Part II: their genesis and implications. *Mon. Weather Rev.* **131**: 2804–2823.

Trier S, Davis C, Ahijevych D, Weisman M, Bryan G. 2006. Mechanisms supporting long-lived episodes of propagating nocturnal convection within a 7-day WRF model simulation. *J. Atmos. Sci.* **63**: 2437–2461.

Wang S-Y, Chen T-C, Correia J Jr. 2011. Climatology of summer midtropospheric perturbations in the US northern plains. Part I: influence on northwest flow severe weather outbreaks. *Clim. Dyn.* **36**: 793–810.

Wang S-Y, Chen T-C, Taylor SE. 2009a. Evaluations of NAM forecasts on midtropospheric perturbation-induced convective storms over the US northern plains. *Weather Forecast.* **24**: 1309–1333.

Wang SY, Gillies RR, Takle ES, Gutowski WJ. 2009b. Evaluation of precipitation in the Intermountain Region as simulated by the NARCCAP regional climate models. *Geophys. Res. Lett.* **36**: L11704, DOI: 10.1029/2009GL037930.

Weisman ML. 1993. The genesis of severe, long-lived bow echoes. *J. Atmos. Sci.* **50**: 645–670.

Weisman ML, Skamarock WC, Klemp JB. 1997. The resolution dependence of explicitly modeled convective systems. *Mon. Weather Rev.* **125**: 527–548.

Weisman ML, Trapp RJ. 2003. Low-level mesovortices within squall lines and bow echoes. Part I: overview and dependence on environmental shear. *Mon. Weather Rev.* **131**: 2779–2803.

Yoon JH, Ruby Leung L, Correia J. 2012. Comparison of dynamically and statistically downscaled seasonal climate forecasts for the cold season over the United States. *J. Geophys. Res.* **117**: D21109, DOI: 10.1029/2012JD017650.

Zhao L, Jin J, Wang SY, Ek MB. 2012. Integration of remote-sensing data with WRF to improve lake-effect precipitation simulations over the Great Lakes region. *J. Geophys. Res.* **117**: D09102, DOI: 10.1029/2011JD016979.

